ISSN 3033-2559
OPEN ACCESS
DOI : https://doi.org/10.29114/ejtuv.vol1.iss3.79

СРАВНИТЕЛЕН АНАЛИЗ НА РАБОТАТА НА АСИНХРОНЕН ДВИГАТЕЛ И СИНХРОНЕН РЕАКТИВЕН ДВИГАТЕЛ ПРИ ЗАДВИЖВАНЕ НА ПРОМИШЛЕН БУТАЛЕН КОМПРЕСОР

Гл. ас. д-р инж. Христиан Панчев
Технически университет - Варна

Резюме: *Принципът на действие на синхронния реактивен двигател (SRM) е известен още от началото на XIX век. Тези двигатели навлязоха в промишлеността едва наскоро, тъй като специфичният им принцип на работа изискваше специализирани устройства за управление – устройства, чието създаване стана възможно благодарение на развитието на силовата електроника. Поради конструктивните си особености, синхронните реактивни двигатели се отличават с висока ефективност, но изискват използването на честотни регулатори (VFD). В настоящия доклад се сравнява енергийната ефективност на система, състояща се от синхронен реактивен двигател и честотен регулатор, с тази на стандартен асинхронен двигател.*
Ключови думи: Синхронен реактивен двигател, честотен регулатор, енергийна ефективност

COMPARATIVE ANALYSIS OF THE OPERATION OF AN ASYNCHRONOUS INDUCTION MOTOR AND A SYNCHRONOUS RELUCTANCE MOTOR DRIVING AN INDUSTRIAL RECIPROCATING COMPRESSOR

Assoc. Prof. Dr. Eng. Hristian Panchev
Technical University - Varna

Abstract: *The principle of operation of Synchronous Reluctance Motor (SRM) has been known since about 1800-th year. Only recently, these motors have been introduced into the industry, as they required special type of devices for control, due to their working principle. Such devices are possible thanks to the development of power electronics. Due to their design, SRMs are highly efficient but demand Variable Frequency Drives (VFD). This report compares the operation of the VFD-SRM kit and a standard induction motor in terms of power efficiency.*
Keywords: Synchronous Reluctance Motor, Variable Frequency Drive, Power Efficiency

1. Introduction

With the growth of technical progress, the problem of the development of energy-saving technologies is becoming more and more acute worldwide. The problem is serious and is related not so much to the growth of electricity consumption in industry and households or to the need to commission new power plants, but to the limited global reserves of natural resources and

е-списание ТУ-Варна
ISSN 3033-2559
OPEN ACCESS
DOI : https://doi.org/10.29114/ejtuv.vol1.iss3.79

environmental pollution. In addition, it is known that the main share of electricity consumption is occupied by electric drives.

The analysis of the production of world manufacturers of electric drives and scientific articles in this field allows us to note the following pronounced trend in the development of electric drives – a steady decrease in the share of uncontrolled electric drives and increase the share of controlled ones.

This is related to the increased requirements of technological processes as well as to the savings of electricity and the related reduction of greenhouse gases. The desire for ever-increasing efficiency of electric drives is reflected in the development of new and better controls, as well as in the designs of various types of motors. The tendency is to choose the type of electric drive specially and individually for the specific type of task. This drive for higher efficiency is also reflected in various government standards. In the United States, EISA (the Energy Independence and Security Act) came into force in 2010 and imposes higher standards for three-phase asynchronous motors with a general purpose of 1 to 500 horsepower. There are similar regulations in Europe. Since June 2011, the European Union only allows motors with efficiency class IE2 (International Efficiency), which is 7% more than older IEC designs. From 2017, only engines with efficiency class IE3 will be allowed in the European Union. Motors with this efficiency class are 10% more efficient than older IEC designs, which now gives them economic meaning due to their energy saving potential. At some point, however, the law of reducing returns began to emerge. With motors running in the efficiency range of 90% and more for a long power range, there is not much more room for improvement. The laws of physics make it impossible to design asynchronous motors with higher efficiency. Here the application of other types of electric motors begin to make sense.

Other types of motors are already on the market and in many cases the replacement of an induction motor with its control with another type of motor with its control is appropriate. At the same time, the methods for selecting an induction motor are well known and workable, while the problem of selecting, for example, a reactive electric motor with its corresponding control is not sufficiently clear. The control of these motors allows the programming of the mechanical characteristics (the relationship between speed and torque) so that they coincide with the mechanical characteristics of the driven load in real time, of course in the temperature range and the maximum torque of the engine.

The literature gives an example of reprogramming the control so that from an engine developing a constant torque, it becomes a motor with a high starting torque. Due to the fact that these engines operate in a wide range of developed speeds and torque, the need for transmissions between the engine and the driven machine is often eliminated.

The asynchronous motor has been the workhorse of the industry since its inception in 1887 by Nikola Tesla. Thanks to the continuous improvements of the induction motor, "a 100-horsepower induction motor currently has the same mounting dimensions as a 7.5-horsepower motor in 1897" (Wikipedia). The principle of operation of Synchronous Reluctance Motor (SRM) has been known since about 1800-th year. Only recently, these motors have been introduced into the industry, as they required special type of devices for control, due to their working principle. Such devices are possible thanks to the development of power electronics. Due to their design, SRMs are highly efficient but demand Variable Frequency Drives (VFD).

ТЕХНИЧЕСКИ УНИВЕРСИТЕТ - ВАРНА
Technical University of Varna
е-списание ТУ-Варна
ISSN 3033-2559
OPEN ACCESS
DOI : https://doi.org/10.29114/ejtuv.vol1.iss3.79

Modern power supply systems are characterized by high dynamics and powerful nonlinear loads. This in turn leads to non-stationary electromagnetic processes and a complex situation regarding electromagnetic compatibility. As a rule, all this leads to increased electricity losses and reduced energy efficiency.

2. Experimental setting

The experimental setup is shown on Fig. 1. The motors shown in Fig. 1 (left and right) drive an industrial reciprocating compressor.

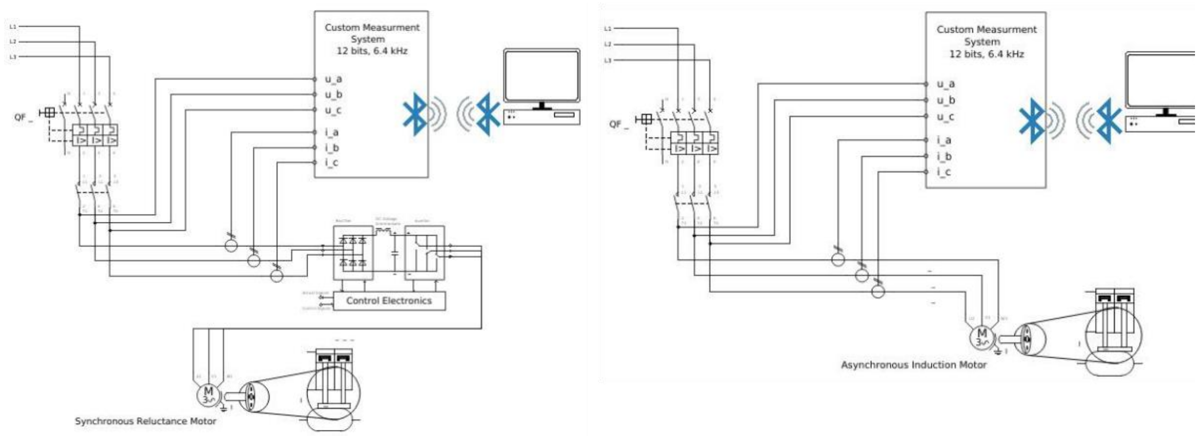

Fig. 1. Experimental setup. left – with synchronous reluctance motor and variable frequency driver, right – with asynchronous induction motor

The squirrel-cage induction motor (shown on Fig. 1 on the right) tested in the laboratory has a 5.5 kW rated power, 400V rated voltage, 50Hz rated frequency and 2910 rated rpm with efficiency class IE2 and efficiency 85%.

The synchronous reluctance motor (shown on Fig. 1 on the left) tested in the laboratory has a 5.5 kW rated power, 400V rated voltage, 50Hz rated frequency and 1500 rated rpm with efficiency class IE5 and efficiency 93.7%. The variable frequency drive shown on Fig.1 on the left is made from same manufacturer who made the synchronous reluctance motor.

This industrial piston compressor (shown on Fig. 2) has two cast iron cylinders. The electric motor transmits movement to the belt pulley of the piston air compressor by two belts. The belt pulley of the compressor serves both as a flywheel and as a fan. The compressor is equipped with a tank with a volume of 270 liters at performance of 827 [l/min]. The rated crankshaft speed of the compressor is 1250 rpm and the maximal pressure in the tank is 11 bar. The weight of the compressor system is 210 kg. Fig. 1.

The custom measurement system (shown in Fig. 1) is made by associate professor V. Chikov, from same department, and it has the following features: resistive dividers for the input voltages, current transformers for the currents, analog to digital converter(ADC) with 12 bits resolution and sampling frequency of6.4 [kHz], suitable for DWPT. This device also has a microcontroller for controlling the ADC, saving the data in temporary buffers and Bluetooth communication with personal computer.

On the personal computer, the data are processing with custom made software. The data itself are the instantaneous values of the electrical quantities that are measured.

ТЕХНИЧЕСКИ УНИВЕРСИТЕТ - ВАРНА
Technical University of Varna
е-списание ТУ-Варна
ISSN 3033-2559
OPEN ACCESS
DOI : https://doi.org/10.29114/ejtuv.vol1.iss3.79

For the data processing, the Python3 (Python) scripting language is used, with the auxiliary libraries which forming suitable environment for data analysis [7],[8],[9],[10] and plotting [11].

Fig 2. Piston air compressor under test

3. Experimental results

On Fig.3 on the left, the instantaneous values for the phase voltages and currents for the synchronous reluctance motor, measured according to the scheme shown on Fig.1 on the left, are depicted.

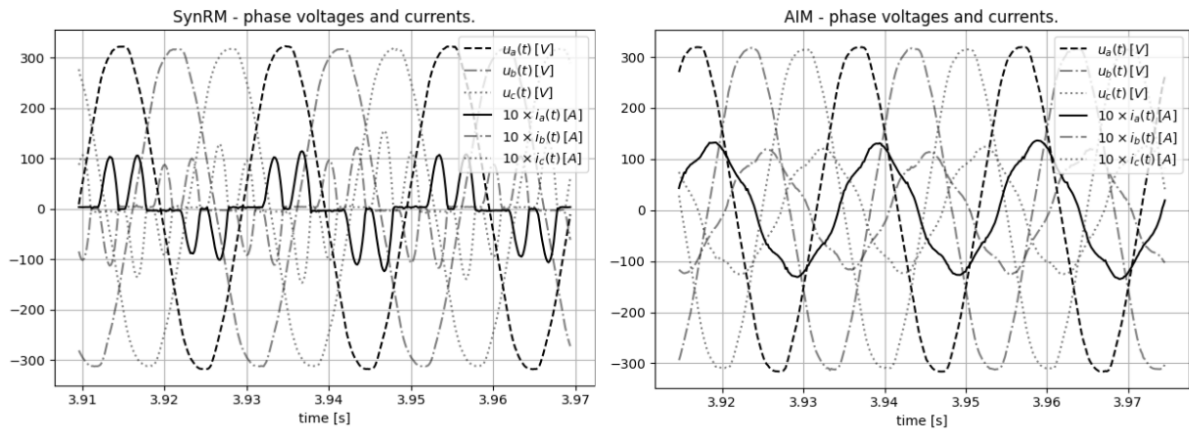

Fig. 3. The phase voltages and currents for the two motors.

On Fig.3 on the right, the instantaneous values for the phase voltages and currents for the asynchronous inductance motor, measured according to the scheme shown on Fig.1 on the right, are depicted.

It can be seen that the voltages in both experiments have approximately the same values and shape. The shape of the current of the SynRM - VFD set is due to the fact that there is an uncontrollable three-phase bridge rectifier at the input of the VFD. The shape of the current of the induction motor is due to the interaction of the harmonics in the supply voltage with the motor, as well as the impedance of the supply line, from the measuring point to the motor.

ISSN 3033-2559
OPEN ACCESS
DOI : https://doi.org/10.29114/ejtuv.vol1.iss3.79

A characteristic feature of the operation of various types of reciprocating compressors widely used in both industrial and marine electrical equipment are the generated current subharmonics, which can lead to the appearance of subharmonics in the voltage at the terminals of other users connected on the same bus. In the sources [1] and [3], the relationship between the electromagnetic torque in the air gap of an induction motor due to harmonics in the voltage and the current is studied. It is shown that the harmonics on the electrical side of the machine generate pulsating electromagnetic torque. More important is that the authors of these studies have also investigated how the ripple in the torque of the load is reflected in the harmonic spectrum of the stator current.

In Fig. 4 the instantaneous power by phases and the total instantaneous power for both motors, is depicted. The figure shows that the average value of the instantaneous power of the induction motor is higher than that of the SynRM, but its peaks in the SynRM are much higher than those in the induction motor. In addition, the exchange of nonactive power in the induction motor and the lack of it in the SynRM can be seen.

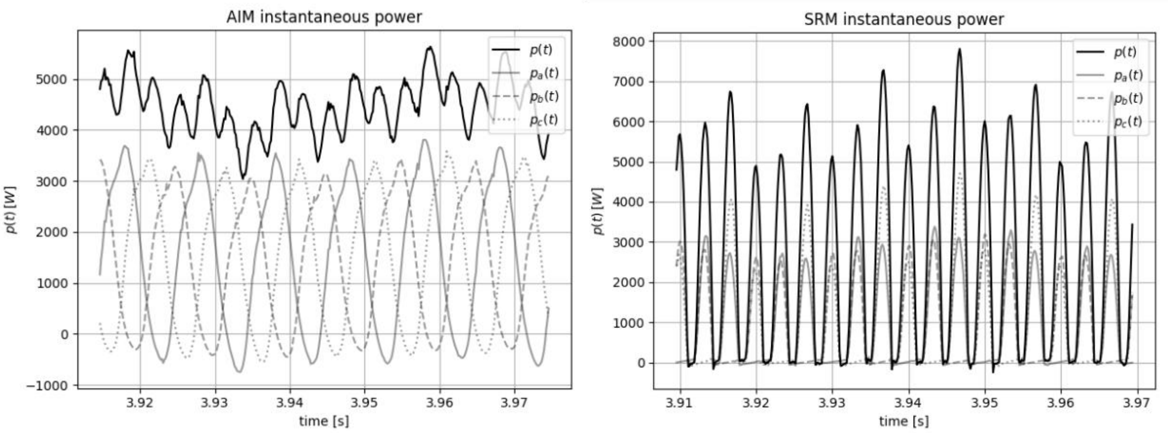

Fig. 4. The instantaneous power for the two motors

On Fig. 5, the Fourier series for the phase voltages and the currents, shown in the Fig. 3, for the two kinds of motors, are depicted. In the harmonic current spectrum of both machines, the characteristic components due to the pulsating torque of the reciprocating compressor are clearly visible. Detailed research on this issue has been published in [4]. This report experimentally proved the existence of two pulsating torques with frequencies of 20 and 40 Hz.

Their corresponding current harmonics with frequencies of 10 and 90 Hz and 30 and 70 Hz are clearly visible in Fig. 5. The same figure shows the same harmonic composition of the supply voltage, which is an indicator that the two experiments were performed under the same conditions. Another less characteristic harmonic in the current spectrum is the third. It can be seen that it is present in the current spectrum of both machines, and in SynRM it is slightly larger. The third harmonic of the current is due to the presence of a third harmonic in the supply voltage. In general, it is clear that the spectral composition of the current of the SynRM is richer in higher harmonics than the spectral composition of the induction motor. The numbers of these harmonics are given by $6k\pm 1$ and are due to the uncontrolled three-phase bridge rectifier at the input of the variable frequency control. The fifth harmonic in the current spectrum of the

ISSN 3033-2559
OPEN ACCESS
DOI : https://doi.org/10.29114/ejtuv.vol1.iss3.79

induction motor is due to the presence of the fifth harmonic in the spectrum of the supply voltage.

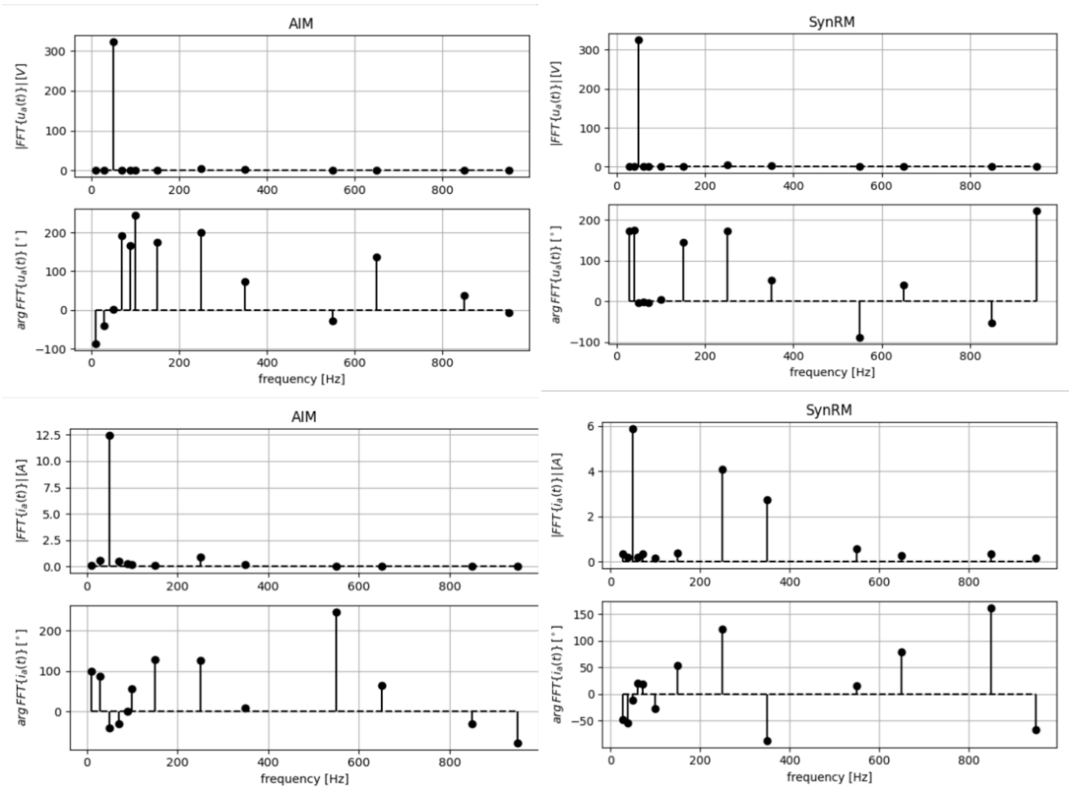

Fig. 5. Fourier series for the phase voltages and currents for the two motors

4. Analysis of the experimental results

The analysis of the powers and the corresponding quantitative and qualitative coefficients are calculated according to the definitions given in the IEEE standard 1459-2010 (IEEE, 2010) and the latest additions to it [6]. All subsequent expressions in this report are according to the definitions given in [6].

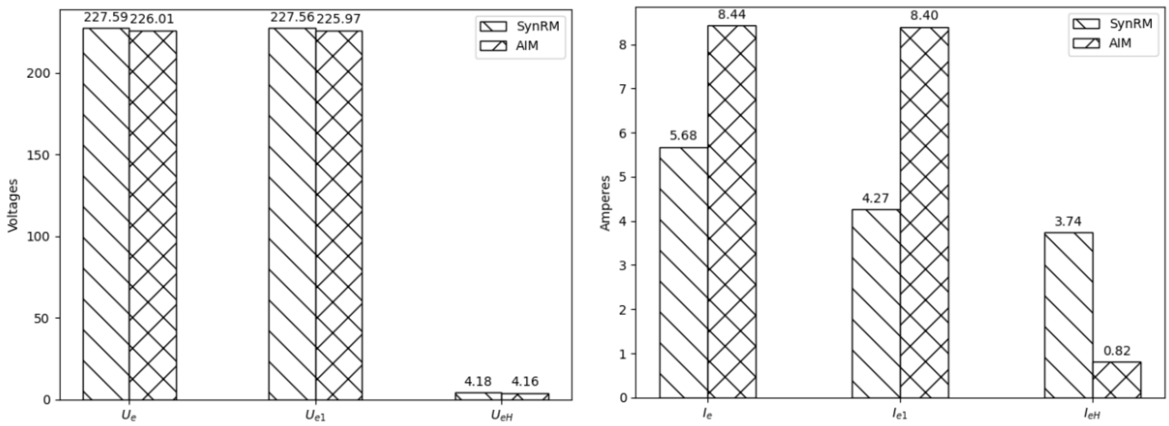

Fig. 6. Effective voltage (Ue), effective current (Ie), fundamental effective voltage (Ue1), fundamental effective current (Ie1), non-fundamental effective voltage (UeH) and non-fundamental effective current (IeH)

ISSN 3033-2559
DOI : https://doi.org/10.29114/ejtuv.vol1.iss3.79

$$
\begin{aligned}
U_e &= \sqrt{\frac{U_a^2+U_b^2+U_c^2}{3}} & I_e &= \sqrt{\frac{I_a^2+I_b^2+I_c^2}{3}} \\
U_{e1} &= \sqrt{\frac{U_{a1}^2+U_{b1}^2+U_{c1}^2}{3}} = \sqrt{\left(U_1^+\right)^2+\left(U_1^-\right)^2+\left(U_1^0\right)^2} & I_{e1} &= \sqrt{\frac{I_{a1}^2+I_{b1}^2+I_{c1}^2}{3}} = \sqrt{\left(I_1^+\right)^2+\left(I_1^-\right)^2+\left(I_1^0\right)^2} \\
U_{eH} &= \sqrt{\frac{U_{aH}^2+U_{bH}^2+U_{cH}^2}{3}} & I_{eH} &= \sqrt{\frac{I_{aH}^2+I_{bH}^2+I_{cH}^2}{3}}
\end{aligned}
\qquad (1)
$$

In Fig. 6 it can be seen that the effective supply voltages are practically the same for both the SynRM and the asynchronous motor. This confirms the conclusions made for Fig.3. From the same figure, one can see that the non-fundamental effective current for the SynRM is much higher than the non-fundamental effective current for the AIM. This also confirms the conclusions made for Fig.3.

On Fig.7 fundamental zero-, positive-, and negative-sequence voltage (U_f^0, U_f^+, and U_f^- respectively) and current (I_f^0, I_f^+, and I_f^- respectively) components are depicted. In this figure on the left we again see practically the same composition of the sequences of the fundamental component of the supply voltage for the two experiments. It can be seen that the zero-sequence current is slightly higher at SynPM, while the negative-sequence current is slightly higher at AIM.

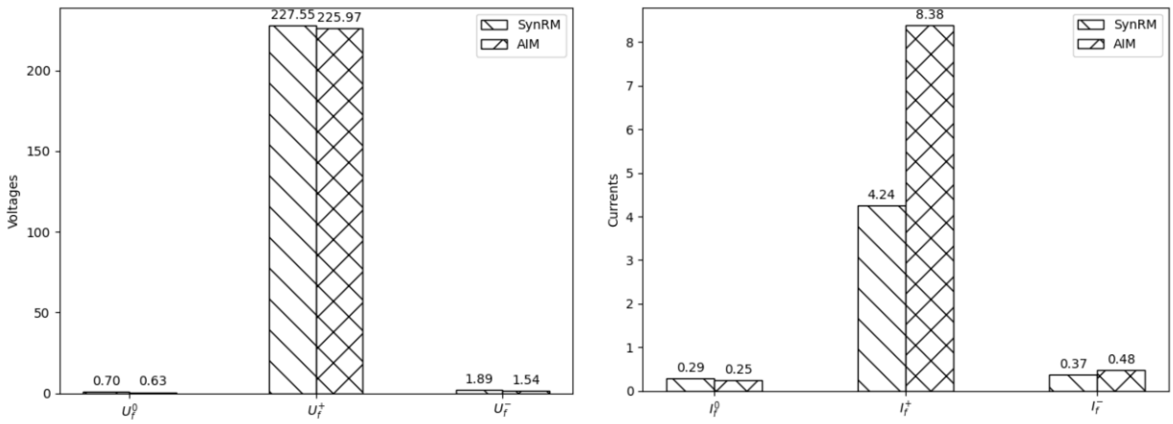

Fig. 7. Fundamental zero-, positive-, and negative-sequence voltage components (U_f^0 ,U_f+, and U_f- respectively) and fundamental zero-, positive-, and negative-sequence current components (I_f^0 , I_f+, and I_f- respectively)

On Fig. 8 various kind of powers calculated by means of the definitions in (Munoz-Galeano, 2015) are depicted.

$$
\begin{aligned}
P &= \sum_{k=1}^{m}\sum_{h} U_{kh} I_{kh} \cos\varphi_{kh} & S_{e1} &= 3U_{e1}I_{e1} \\
P_f^+ &= \sum_{k=1}^{m} U_k I_k \cos\varphi_k & S_f^+ &= \sqrt{\left(P_f^+\right)^2+\left(Q_f^+\right)^2} \\
P_H &= \sum_{k=1}^{m}\sum_{h\neq 1} U_{kh} I_{kh} \cos\varphi_{kh} & S_{U1} &= \sqrt{\left(S_{e1}\right)^2-\left(S_f^+\right)^2} = \sqrt{\left(S_{U1V}\right)^2+\left(S_{U1I}\right)^2+\left(S_{U1U}\right)^2} \\
Q_f^+ &= \sum_{k=1}^{m} U_k I_k \sin\varphi_k & S_{U1V} &= \sqrt{9\left(U_{U1}\right)^2\left(I_f^+\right)^2} \\
S_e &= 3U_eI_e = \sqrt{U_a^2+U_b^2+U_c^2}\sqrt{I_a^2+I_b^2+I_c^2} & S_{U1I} &= \sqrt{9\left(U_f^+\right)^2\left(I_{U1}\right)^2}
\end{aligned}
\qquad (2)
$$

ISSN 3033-2559
OPEN ACCESS
DOI : https://doi.org/10.29114/ejtuv.vol1.iss3.79

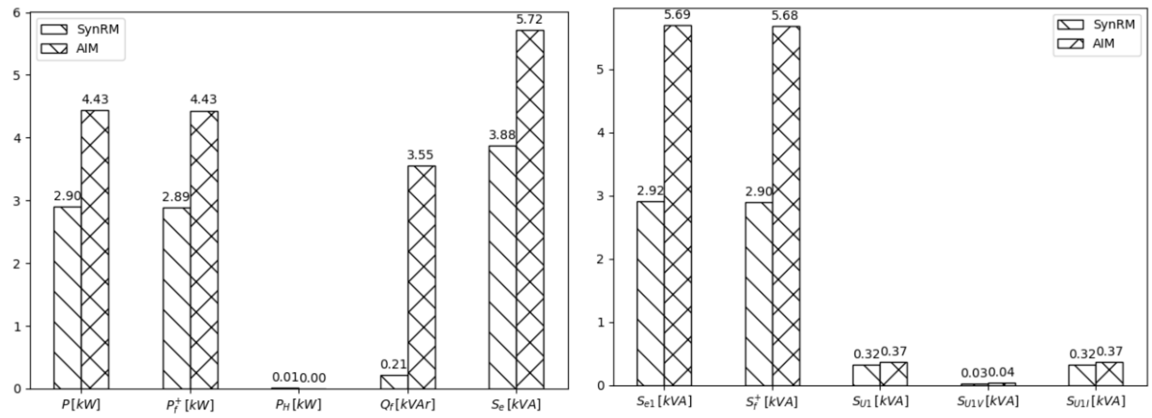

Fig. 8. left – Active power P [kW], Fundamental active power P_f^+ [kW], Harmonic active power PH [kW], Fundamental reactive power Q_f [kVAr], Effective apparent power S_e [kVA] right – Fundamental effective apparent power S_{e1} [kVA], Fundamental positive-sequence apparent power Sf + [kVA], Unbalance power, S_{UI} *[kVA]*, Voltage unbalance power S_{UIV} *[kVA]* and Current unbalance power S_{UII} *[kVA]*

In (2), *k* is the phase number, *m* = 3 is the number of phases, *h* is the harmonic number. In (2), U_{UI} [V] is the unbalance voltage and I_{UI} [A] is the unbalance current.

$$U_{U1} = \sqrt{U_{e1}^2 - \left(U_f^+\right)^2} = \sqrt{\left(U_f^-\right)^2 + \left(U_f^0\right)^2} \qquad I_{U1} = \sqrt{I_{e1}^2 - \left(I_f^+\right)^2} = \sqrt{\left(I_f^-\right)^2 + \left(I_f^0\right)^2} \tag{3}$$

The induction motor draw much more fundamental reactive power as one can see on Fig. 8. As can be seen from Fig. 9, SinRM draws much more non-fundamental effective apparent power from AIM. As can be seen from (4), this power consists of the harmonic apparent power, voltage distortion power and current distortion power. Current distortion power is much higher for the SynRM, because of the uncontrolled three-phase bridge rectifier. Thus the shape of the current and accordingly current distortion power is the reason for the large value of the nonfundamental effective apparent power.

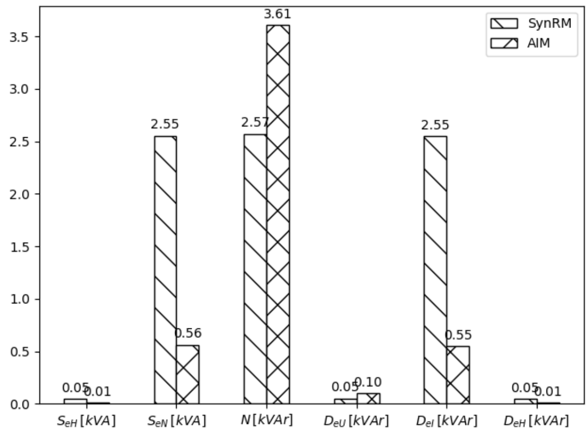

Fig 9. Harmonic apparent power S_{eH} [kVA], Non-fundamental effective apparent power S_{eN} [kVA], Non-active power N [kVAr], Voltage distortion power D_{eU} [kVAr], Current distortion power D_{eI} [kVAr], Harmonic distortion power D_{eH} [kVAr]

ТЕХНИЧЕСКИ УНИВЕРСИТЕТ - ВАРНА
Technical University of Varna
е-списание ТУ-Варна
ISSN 3033-2559
OPEN ACCESS
DOI : https://doi.org/10.29114/ejtuv.vol1.iss3.79

$$S_{eH} = 3U_{eH}I_{eH} = \sqrt{P_H^2 + D_{eH}^2} \qquad D_{eU} = 3U_{eH}I_{e1}$$
$$S_{eN} = \sqrt{D_{eI}^2 + D_{eU}^2 + S_{eH}^2} \qquad D_{eI} = 3U_{e1}I_{eH} \tag{4}$$
$$N = \sqrt{S_e^2 - P^2} \qquad D_{eH} = \sqrt{S_{eH}^2 - P_H^2}$$

On Fig. 10 qualitative indicators for the quality of electricity are depicted.

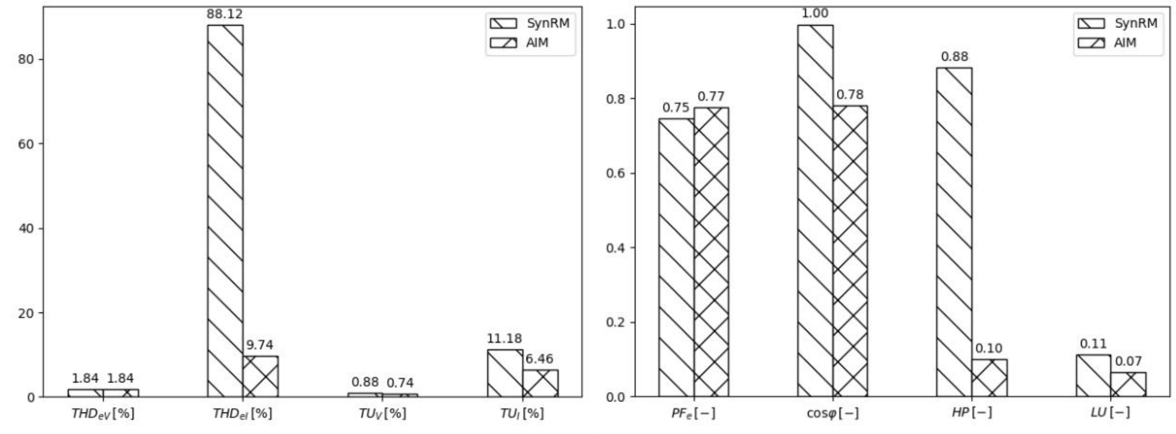

Fig. 10. left – Equivalent total harmonic distortion for voltage THD_{eV} [%], Equivalent total harmonic distortion for current THD_{eI} [%], Total voltage unbalance factor TU_V [%], Total current unbalance factor TU_I[%] right – Effective power factor PFe [-], Classical power factor cos φ [-], Harmonic pollution HP [-], Load unbalance LU [-]

These indicators are calculated according to (5).

$$THD_{eV} = \frac{U_{eH}}{U_f^+} \qquad TU_V = \frac{U_{U1}}{U_f^+} \qquad PF_e = \frac{P_f^+}{S_e} \qquad HP = \frac{S_{eN}}{S_f^+}$$
$$THD_{eI} = \frac{I_{eH}}{I_f^+} \qquad TU_I = \frac{I_{U1}}{I_f^+} \qquad \cos\varphi = \frac{P_f^+}{S_f^+} \qquad LU = \frac{S_{U1}}{S_f^+} \tag{5}$$

The indicators of the SynRM which are worse of these of the induction motor are equivalent total harmonic distortion for the current and harmonic pollution. The classical power factor of the SynRM is unity as one can expected.

5 Conclusion

This report compares the operation of the VFD-SRM kit and a standard induction motor in terms of power efficiency. Experiments show that this kit has many advantages over the induction motor. Advantages such as: low starting current, smooth starting, speed regulation. In addition, the VFD provides many other functions such as smartphone control and numerous motor operation settings. Despite these advantages, however, the kit significantly decrease the qualitative indicators of the power and electromagnetic compatibility. If speed control is not required, the induction motor remains probably a better choice. The same result can be expected from the VFD-AIM kit. Care should be taken to assess whether the increased efficiency of SynRM (in this case by about 8%) over AIM is a decisive advantage.

ISSN 3033-2559
OPEN ACCESS
DOI : https://doi.org/10.29114/ejtuv.vol1.iss3.79

Globally, electronic controls of electric motors are irreversibly entering the electrical equipment of industry, marine power systems and electric transport. The conclusion to be drawn is that power electronic devices for controlling electric motors must be designed and controlled in such a way as to draw a symmetrical sinusoidal current with a unity power factor. At the same time, the efficiency and are reliability must be high and the size and the final price low.

References

1. Manguelle, J.S., Ekemb, G., Mon-Nzongo, D.L., Jin, T. and Doumbia, M.L. (2018, December). "A Theoretical Analysis of Pulsating Torque Components in AC Machines With Variable Frequency Drives and Dynamic Mechanical Loads," in IEEE Transactions on Industrial Electronics, vol. 65, no. 12, pp. 9311-9324, 10.1109/TIE.2018.2823681
2. Manguelle, J.S., et al. (2013). “Analytical expression of pulsating torque harmonics due to PWM drives," 2013 IEEE Energy Conversion Congress and Exposition, Denver, CO, pp. 2813-2820, 10.1109/ECCE.2013.6647066
3. Manguelle, J.S., Nyobe-Yome, J. and Ekemb, G. (2010, Jan.-Feb.). "Pulsating Torques in PWM Multi-Megawatt Drives for Torsional Analysis of Large Shafts," in IEEE Transactions on Industry Applications, vol. 46, no. 1, pp. 130-138, 10.1109/TIA.2009.2036515
4. Chikov, V., Makedonski, N., Panchev, H. and Milev, G. (2020). "Experimental study on the impact of reciprocating compressor systems on the power quality in electrical power supply systems.," 2020 12th Electrical Engineering Faculty Conference (BulEF), Varna, Bulgaria, pp. 1-6, 10.1109/BulEF51036.2020.9326052.
5. IEEE Standard Definitions for the Measurement of Electric Power Quantities Under Sinusoidal, Nonsinusoidal, Balanced, or Unbalanced Conditions. (2010, Mar.). 3 Park Avenue, New York, USA : IEEE Power & Energy Society
6. Munoz-Galeano, N., Alfonso-Gil, J., Grau-Orts, S., Segui-Chillet, S., Gimeno-Sales, F.J. (2015). “Instantaneous approach to IEEE Std. 1459 power terms and quality indices.”, Electrical Power and Energy Systems, Elsevier
7. Walt, S., Colbert, S., & Varoquaux, G. (2011, March-April). The NumPy Array: A Structure for Efficient Numerical Computation, Computing in Science & Engineering, Volume 13, Issue 2, Pages 22-30
8. Jones, E., Oliphant, E., Peterson, P., et al. (2001). SciPy: Open Source Scientific Tools for Python.
9. Perez, F., Granger, B. (2007, May-June). IPython: A System for Interactive Scientific Computing, Computing in Science & Engineering, Volume 9, Issue 3, Pages 21-29
10. McKinney, W. (2010). Data Structures for Statistical Computing in Python, Proceedings of the 9th Python in Science Conference, Pages 51-56
11. Hunter, J. (2007, May-June) Matplotlib: A 2D Graphics Environment, Computing in Science & Engineering, Volume 9, Issue 3, Pages 90-95